RASopathy Mutations Demonstrate the Critical Function of the Cysteine-rich Domain in Maintaining BRAF in an Autoinhibited State

Russell Spencer-Smith[1], Elizabeth M. Terrell[1], Christine Insinna[1], Constance Agamasu[2], Morgan E. Wagner[2], Daniel A. Ritt[1], Jim Stauffer[1], Andrew G. Stephen[2], and Deborah K Morrison[1*]

[1]Laboratory of Cell and Developmental Signaling, Center for Cancer Research, National Cancer Institute-Frederick, Frederick, MD 21702; [2] National Cancer Institute RAS Initiative, Cancer Research Technology Program, Frederick National Laboratory for Cancer Research, Leidos Biomedical Research, Inc., Frederick, MD 21702

[*]Corresponding Author and Lead Contact:

Email: morrisod@mail.nih.gov

Phone: 301-846-1733

Fax: 301-846-1666

BRAF is frequently mutated in human cancer and the RASopathy syndromes, with RASopathy mutations often observed in the cysteine-rich domain (CRD). Although the CRD is known for roles in phosphatidylserine (PS) binding, the RAS-RAF interaction, and RAF autoinhibition, how these differing activities impact BRAF function in normal and disease states is not well-characterized. Here, we analyze a panel of BRAF-CRD mutations and find that they can be classified into three groups based on their ability to relieve autoinhibition and/or enhance PS binding, with relief of autoinhibition being the predominant factor determining mutation severity. Comparison of the BRAF and CRAF CRDs further reveals that the BRAF-CRD is a stronger mediator of both autoinhibition and PS binding. Moreover, given the increased catalytic activity of BRAF versus CRAF, our findings indicate a more critical role for CRD-mediated autoinhibition in BRAF regulation, consistent with the high frequency of mutations that disrupt this function in the RASopathies.

KEY WORDS

BRAF, CRAF, cysteine-rich domain, CRD, autoinhibition, phosphatidylserine, RAS, RASopathies

INTRODUCTION

RAF family kinases (ARAF, BRAF, and CRAF) are essential members of the pro-proliferative/anti-apoptotic RAS-ERK MAPK pathway and function as direct effectors of activated RAS. Under normal signaling conditions, the RAF kinases cycle between three major states[1, 2]: 1) an autoinhibited, monomeric conformation that localizes to the cytosol[3, 4]; 2) an activated, RAS-bound dimeric configuration at the plasma membrane[5, 6]; and 3) a signaling-incompetent monomeric form that has been inactivated and released from the membrane via signal-induced feedback phosphorylation[7, 8]. This regulatory cycle can be disrupted by mutational events to promote upregulated RAF signaling in human disease states such as cancer and the RASopathy syndromes[9].

The RASopathies are a group of related developmental disorders caused by germline mutations in components of the RAS-ERK MAPK pathway[10]. These disorders, which include cardiofaciocutaneous (CFC), Costello, and Noonan syndromes, are characterized by distinct craniofacial abnormalities, developmental delays, cardiac defects, and an increased risk of certain childhood cancers[11]. With regard to the RAF kinases, RASopathy mutations are observed in both *BRAF* and *CRAF* but tend to occur in different regions of the proteins and are primarily associated with distinct RASopathy syndromes[12-15]. In particular, germline alterations in *BRAF* are mainly observed in CFC syndrome (75% of CFC cases) and frequently occur in the cysteine-rich domain (CRD; ~38% of mutations)[14, 15], a zinc-finger domain found in the N-terminal regulatory region of all RAF kinases.

Prior studies characterizing the RAF CRDs have established roles for the CRD as both a facilitator of RAF activation under signaling conditions[16, 17], through interactions with phosphatidylserine (PS) in the plasma membrane[18-20]and/or direct RAS contact[21-25], and as a mediator of autoinhibitory interactions during quiescent conditions[4, 26-28]. However, the interplay between these opposing activities and their relative importance in modulating the function of individual RAF members is not well-understood. Here, analysis of a panel of RASopathy-associated BRAF-CRD mutations provides key insights regarding BRAF regulation and reveals functional differences between RAF members that are relevant to the molecular etiology of the RASopathies.

RESULTS

Effect of RASopathy-associated BRAF-CRD mutations on phosphatidylserine binding. RASopathy-associated mutations in the BRAF-CRD can be broadly divided into two groups – those that cluster in and around Loop 1 (hereon referred to as L1 mutations; Fig. 1a and Supplementary Fig. 1) and those found downstream of L1 that introduce additional positively charged residues into the CRD (referred to as PC mutations), with Q257R being the most common CRD mutation (Fig. 1a). To determine how the CRD mutations impact BRAF function, a panel of L1 (T241P, T241R, A246P) and PC (Q257R, Q262K and E275K) mutants were selected for investigation. Given that a well-established property of the RAF CRDs is their ability to interact with PS, which contributes to the membrane recruitment of RAF for kinase activation, we first examined the effect of the CRD mutations on PS binding. For these experiments, surface plasmon resonance (SPR) was used to monitor the binding of isolated WT or mutant BRAF-CRD proteins (amino acids 232-284) to nanodiscs or liposomes that lacked (100%POPC) or contained PS (20%POPS:80%POPC). As expected, the WT-CRD exhibited preferential binding to the nanodiscs and liposomes that contain PS (Fig. 1b and Supplementary Fig. 2), with binding reduced ~80% to the lipid surfaces that lacked PS. No significant change in binding was observed for CRDs containing the L1 mutations. In contrast, binding to the PS-containing nanodiscs and liposomes was increased for CRDs containing the PC mutations, with the Q257R-CRD demonstrating the highest level of interaction as reflected in the normalized binding slopes for the Nanodisc-binding assays and in the partition coefficients for the liposome-binding assays (Fig. 1c,d). Finally, when the isolated CRD proteins were fused to GFP and their localization examined in COS-7 cells, the fusion proteins could be detected at the cell periphery, and this localization correlated with the PS binding activity observed in the SPR analysis (Fig. 1e-f).

Effect of RASopathy-associated BRAF-CRD mutations on RAF autoinhibitory interactions. The CRD is also known to play a role in RAF autoinhibition, which must be relieved for kinase activation to occur. To assess RAF autoinhibition, a proximity-based NanoBRET assay[29] was developed in which RAF autoinhibitory interactions could be quantified under live cell conditions.

Previous studies have shown that when co-expressed as separate proteins, the isolated RAF regulatory (REG) domain can bind the catalytic (CAT) domain to suppress its signaling activity and that the autoinhibitory function of the REG domain requires an intact CRD[26-28]. Therefore, we generated expression constructs in which $BRAF^{REG}$ (residues 1-435) contained a C-terminal, Halo energy acceptor tag and $BRAF^{CAT}$ (residues 435-766) contained an N-terminal, NanoLuc energy donor tag. When co-expressed in 293FT cells, $BRAF^{REG}$-Halo was found to interact with Nano-$BRAF^{CAT}$, as evidenced by energy transfer and the generation of a BRET signal (Fig. 2a). In addition, $BRAF^{REG}$-Halo could suppress MEK phosphorylation induced by Nano-$BRAF^{CAT}$ in a manner that was dose-dependent and correlated with an increased BRET signal (Fig 2a,b), confirming the validity of the NanoBRET assay as a measure of autoinhibitory interactions.

The NanoBRET assay was also able to detect a relief in autoinhibitory interactions, as co-expression of a potent RAF activator, $KRAS^{G12V}$, resulted in a 40-50% reduction in the BRET signal (Fig. 2c), consistent with the binding of $BRAF^{REG}$ to membrane-localized $KRAS^{G12V}$ and reduced interaction with $BRAF^{CAT}$. In addition, the NanoBRET assay was sensitive to perturbations caused by internal BRAF mutations, as incorporation of the oncogenic V600E mutation into $BRAF^{CAT}$ reduced the BRET signal ~50% (Fig. 2c). When the various CRD mutations were introduced into $BRAF^{REG}$, we found that all L1 mutations, along with PC mutations Q257R and Q262K, caused a significant reduction in the BRET signal, reflecting reduced binding to $BRAF^{CAT}$ (Fig. 2c). In contrast, the E275K mutation, which resulted in enhanced PS binding, had no effect on $BRAF^{CAT}$ interactions (Fig. 2c), indicating that increased PS binding alone is not sufficient to relieve autoinhibition. These findings are in agreement with the published cryo-EM structure of an autoinhibited BRAF monomer bound to dimeric 14-3-3[4], which shows that the PS binding interface of the CRD is occluded in the autoinhibited state and that all of the analyzed CRD mutations, with the exception of E275K, occur in or adjacent to residues that make contact with the BRAF CAT domain and/or 14-3-3 to maintain the autoinhibited conformation (Fig. 2d).

Effect of RASopathy-associated CRD mutations on RAS-RAF binding and BRAF signaling activity. Due to the important role of the plasma membrane in both CRD and RAS function, effects of the CRD mutations on RAS-RAF binding were monitored under live cell conditions using a

traditional BRET assay[30]. For these studies, full-length BRAF tagged with RLuc8 served as the energy donor ($BRAF^{FL}$-RLuc8) and Venus tagged $KRAS^{G12V}$ functioned as the energy acceptor (Venus-$KRAS^{G12V}$). In addition, saturation curves were generated such that the $BRET_{max}$ (the maximal level of RAS binding) and $BRET_{50}$ (the relative affinity of the interaction) could be determined.

As expected, WT-$BRAF^{FL}$ generated a strong BRET signal that was dramatically reduced by incorporation of the RBD R188L mutation that disrupts RAS binding (Fig. 3a,b). Analysis of the CRD mutants revealed that proteins containing mutations that relieve autoinhibition generated a $BRET_{max}$ signal that was increased ~65% over that observed for WT (Fig. 3a,b). In contrast, the E275K mutation, which enhances PS binding but does not relieve autoinhibition, resulted in a markedly weaker increase in the $BRET_{max}$ signal (~21%). Interestingly, when the $BRET_{50}$ values were calculated, all PC mutants, including E275K, exhibited an increase in the affinity of the KRAS interaction (lower $BRET_{50}$ values) (Fig. 3b), suggesting that PS binding may specifically contribute to the affinity of KRAS binding. Indeed, when the BRET assays were conducted using the isolated $BRAF^{REG}$ domain, where autoinhibition would not be a factor, the CRD L1 mutants generated BRET signals that were equivalent to WT-$BRAF^{REG}$ in terms of both the $BRET_{max}$ and $BRET_{50}$ values (Supplementary Fig. 3), consistent with these mutations only affecting autoinhibition. In contrast, an elevated level and affinity of RAS binding was observed for the PC mutants that correlated with the effect of these mutations on CRD-PS binding (Q257R>E275K>Q262K; Supplementary Fig. 3).

The above experiments demonstrate that the RASopathy-associated CRD mutations vary in their effects (Supplementary Table 1), with the L1 mutations causing a relief in autoinhibition (which we refer to as Class A), the PC Q257R and Q262K mutations both relieving autoinhibition and increasing PS binding (Class B), and the PC E275K mutation resulting only in enhanced PS binding (Class C). Moreover, analysis of CRD mutant proteins revealed that relief of autoinhibition alone was sufficient to increase the overall levels of RAS-RAF binding in live cells, whereas enhanced PS binding contributed to the affinity of the interaction, either by stabilizing membrane interactions and/or promoting direct contact between the CRD and RAS. To determine how these differing effects influence the signaling activity of BRAF, BRAF proteins containing the CRD

mutations were evaluated in focus forming assays (Fig. 3c,d, and Supplementary Table 2) using NIH-3T3 cells. As shown in Fig 3d, while no foci were observed on cell monolayers expressing WT-BRAF^{FL}, all of the CRD mutants were able to induce focus formation. Strikingly, the BRAF proteins containing mutations that relieve autoinhibition (Class A and B) were found to be significantly more transforming than was the E275K mutant (Class C), which only exhibits enhanced PS binding (Fig. 3d). When MEK activation in the NIH-3T3 cells was monitored, E275K-BRAF^{FL} was also the weakest at promoting MEK phosphorylation on activating sites (Fig. 3c).

RASopathy-associated mutations in the BRAF-CRD increase the biological activity of BRAF in zebrafish embryos. To investigate the effects of the CRD mutations on BRAF function in a developing organism, the zebrafish model system was used, as expression of RASopathy mutants has been shown to induce defects in zebrafish embryos similar to those observed in RASopathy patients, including alterations in the heart and craniofacial structures[31]. In addition, monitoring the effects of RASopathy mutants on early convergent-extension cell movements, which results in elongated embryos with an abnormal axis ratio, has been used to assess mutation severity[32]. For our studies, a representative of each of the three mutant classes was examined: T241P (Class A), Q257R (Class B), and E257K (Class C). In the convergent extension assay, expression of E257K-BRAF had a more modest effect on the embryo axis ratio than did the T241P or Q257R mutants, resulting in an axis ratio of 1.05 versus 1.13-1.14 for the Class A and B mutants (Fig. 4a). In addition, approximately 26-30% of embryos expressing the T241P or Q257R mutants exhibited enlarged hearts with edema, whereas less than 10% of those expressing E275K-BRAF had heart edema (Fig. 4b). Finally, we examined whether expression of the CRD mutants caused alterations in the development of craniofacial structures by measuring the angle of the ceratohyal, which corresponds to the width and bluntness of the head and is an excellent marker for hypertelorism, a common feature of RASopathy patients. Using the transgenic *Tg (col2a1aBAC:GFP)*[33] zebrafish line to visualize cartilage cells, we found that expression of either the T241P or Q257R mutant caused a significant increase in the angle of the ceratohyal, whereas expression of the E257K mutant did not (Fig. 4c). These functional assays, and the above signaling experiments, indicate that the E275K

substitution is a less severe mutation, a finding consistent with the phenotypic analysis of a CFC patient possessing this mutation, who does not exhibit hypertelorism, short stature, or mental retardation, characteristics frequently observed in CFC patients with BRAF-CRD mutations[34] (Fig. 4d). Notably, these findings suggest that relief in CRD-mediated autoinhibition is the primary factor determining the severity of the RASopathy-associated BRAF-CRD mutations.

The CRDs of BRAF and CRAF differ in their ability to bind PS. Although the BRAF-CRD is frequently mutated in the RASopathies, no RASopathy-associated mutations in the CRAF-CRD have been identified, despite reports that the CRAF-CRD also contributes to autoinhibition, PS binding, and the RAS-RAF interaction[24, 25, 27, 35-37]. Therefore, studies were initiated to compare the properties of the BRAF- and CRAF-CRDs. Through SPR analysis, we found that the CRAF-CRD exhibited specific binding to the 20% POPS/80% POPC nanodiscs, but the level of binding was ~30% of that observed for the BRAF-CRD (Fig. 5a,b and Supplementary Fig. 4). In addition, when the isolated CRD proteins were fused to GFP and their localization examined in COS-7 cells, the BRAF fusion protein was clearly visible at the cell periphery, whereas the isolated CRAF-CRD was observed primarily in the cytosol and nucleus (Fig. 5c). Of note, the nuclear localization of the GFP-CRD is likely due to its small size (33.8 kDa), which would permit diffusion into the nucleus as has been reported for the PKC CRD[38, 39].

To ascertain the residues contributing to the differing PS binding activities of the BRAF- and CRAF-CRDs, we examined the subcellular localization of a series of GFP-tagged CRD proteins in which non-conserved residues between the BRAF and CRAF-CRDs had been exchanged. From this analysis, four BRAF residues (F250, R252, Q270, and R271) were identified that when substituted for the equivalent residues in the CRAF-CRD (4MUT-CRAF, I154F Q156R, E174Q, and H175R) resulted in an enhanced cell surface localization that was comparable to the BRAF-CRD (Fig. 5c). Likewise, inserting the equivalent residues from CRAF into the BRAF-CRD (4MUT-BRAF) caused a significant decrease in localizataion at the plasma membrane (Fig. 5c). SPR analysis further revealed that these changes correlated with the PS binding activity of the CRDs and that the PS binding activity of the BRAF- and CRAF-CRDs could largely be reversed by exchanging these four non-conserved residues (Fig. 5a,b). Interestingly, surface charge

comparisons of the RAF CRD structures revealed that these four residues localize to the top surface of the CRD that contains the membrane binding interface (Fig. 5d). The CRAF residue E174 adds an acidic amino acid to this region, which would be repulsive in the context of the negatively charged plasma membrane, whereas the BRAF residues R252 and R271, together with the conserved lysine at position 253 (K253), form a positively charged patch conducive to PS binding. Notably, the CRD PC mutations would further expand this positively charged patch (Fig. 5e), consistent with these mutations causing enhanced PS binding.

The BRAF-CRD is a more potent mediator of autoinhibition than is the CRAF-CRD. To compare the autoinhibitory activities of the CRDs of BRAF and CRAF, a $BRAF^{REG}$ construct was generated in which the BRAF-CRD was replaced with that of CRAF, following which the ability of the C-CRD-$BRAF^{REG}$ to interact with the $BRAF^{CAT}$ domain was monitored using the NanoBRET assay. In comparison to $BRAF^{REG}$, the BRET signal generated by C-CRD-$BRAF^{REG}$ was significantly lower (Fig. 6a), indicating a reduced ability of the C-Raf-CRD to mediate autoinhibitory interactions. Consistent with this result, when similar constructs were generated to evaluate CRAF autoinhibition, an interaction between the $CRAF^{REG}$ and $CRAF^{CAT}$ domains was observed; however, if $CRAF^{REG}$ contained the BRAF-CRD, the BRET signal was increased approximately 40% (Fig. 6a). In addition, when the $BRAF^{REG}$ proteins were evaluated for binding to $CRAF^{CAT}$ and vice versa, similar results were observed (Fig. 6a), indicating that the increased autoinhibitory activity of the BRAF-CRD is not determined by differences in the BRAF versus CRAF catalytic domains. Next, we examined the effect of the CRAF-CRD in the context of full-length $BRAF^{FL}$ and found that exchanging the BRAF-CRD for that of CRAF increased the levels of RAS-RAF binding in the live cell BRET assay, consistent with a reduced autoinhibitory activity for the CRAF-CRD (Fig. 6b). In addition, we found that C-CRD-$BRAF^{FL}$, but not WT-$BRAF^{FL}$, was able to induce focus formation on NIH-3T3 monolayers (Fig. 6c and Supplementary Table 2), further demonstrating the function of the BRAF-CRD in maintaining BRAF in an autoinhibited, non-signaling state.

Although both the PS binding and autoinhibitory activities of the BRAF-CRD were elevated in comparison to the CRAF-CRD, we found that the four non-conserved BRAF residues

contributing to enhanced PS binding were not critical for the elevated autoinhibitory activity of the BRAF-CRD, as 4MUT-BRAF^{REG} showed no impairment in binding BRAF^{CAT} in the NanoBRET assay (Fig. 6d). Through the analysis of a series of BRAF^{REG} proteins in which non-conserved residues between the BRAF- and CRAF-CRDs were exchanged, a single residue swap in L1, T244K (K149 in CRAF), was found to reduce interactions between BRAF^{REG} and BRAF^{CAT} in the NanoBRET assay to a level observed with C-CRD-BRAF^{REG} (Fig. 6d). Interestingly, in the autoinhibited structure of the BRAF monomer, T244 lies in close proximity to R719 in the BRAF catalytic domain[4] and placement of a lysine residue at position 244 would likely generate repulsive forces with R719, thereby destabilizing the autoinhibitory contacts of the CRD (Fig. 6d). Finally, when the effect of the T244K substitution was examined in focus forming assays, we found that T244K-BRAF^{FL}, but not 4MUT-BRAF^{FL}, was as transforming as C-CRD BRAF^{FL} (Fig 6c and Supplementary Table 2).

Analysis of CRAF Proteins Containing Mutations Analogous to the RASopathy BRAF-CRD Mutations. Given that the basal catalytic activity of BRAF is significantly higher than that of CRAF, due largely to the constitutive negative charge of the N-region (residues 444-449) in the BRAF kinase domain[40, 41]; the enhanced autoinhibitory activity of the BRAF-CRD may be specifically required to quell the high basal catalytic activity of BRAF and may account for the lack of RASopathy-associated mutations in the CRAF-CRD. To investigate this possibility, constructs expressing full-length CRAF that contained CRD mutations equivalent to T241P, Q257R, and Q262K (CRAF T145P and N161R, and Q166K) were generated and examined for their focus forming potential. As shown in Fig. 7a, none of these mutants could induce foci. However, when the N-region of these CRAF mutants was changed to that of BRAF, conferring high basal catalytic activity (Fig. 7b), the CRAF-CRD mutants were now transforming (Fig. 7a and Supplementary Table 2). Moreover, a CRAF protein containing only the BRAF N-region sequences were also weakly transforming, consistent with elevated catalytic activity of the hybrid protein and the reduced autoinhibitory activity of the CRAF-CRD. These findings suggest that CRD-mediated autoinhibition may play a more critical role in BRAF regulation, functioning to maintain BRAF in an inactive state during non-signaling conditions.

DISCUSSION

Early investigation of the RAF kinases demonstrated the role of the CRD in PS binding, the RAS-RAF interaction, and autoinhibition; however, the importance of these activities in terms of RAF regulation and biological function have not been well explored. Through our studies, we find that the BRAF-CRD is a stronger mediator of both PS binding and autoinhibition than is the CRAF-CRD and that the RASopathy-associated BRAF-CRD mutations can be classified into three functional groups: Class A, causing relief in autoinhibition; Class B, relieving autoinhibition and enhancing PS binding; and Class C, enhancing PS binding alone. Strikingly, the ability of the mutations to alter distinct activities of the CRD was found to have direct consequences on the RAS-binding properties of BRAF and on its biological output, further elucidating how specific CRD functions contribute to BRAF regulation.

Analysis of the BRAF-CRD mutants revealed that relief of autoinhibition alone was sufficient to robustly increase the overall levels of RAS-RAF binding, whereas enhanced CRD-PS binding contributed to the affinity of the RAS-RAF interaction, either through membrane interactions or by facilitating direct contact with RAS. In addition, the BRAF-CRD mutants with impaired autoinhibitory activity (Class A and B) were significantly more transforming in focus forming assays, were stronger mediators of MEK activation, and caused more pronounced developmental defects when expressed in zebrafish than was observed for the Class C E275K mutant, which only exhibits enhanced PS binding. Taken together, these functional assays suggest that relief of CRD-mediated autoinhibition is the primary factor determining the severity of the RASopathy-associated CRD mutation. It is interesting to note that the evaluation of one RASopathy patient with the Class C E257K mutation has been reported and this patient does not display several attributes reported for all patients possessing Class A T241P and Class B Q257R mutations, such as hypertelorism, short stature, and development delays[34] (Fig. 4d). Although the number of patient reports available is quite limited, the NanoBRET assay to measure RAF autoinhibition and the functional assays described here may be particularly useful in predicting the severity of new BRAF-CRD mutations as they are identified through various ongoing and future genomic sequencing projects.

In this study, we also compared the properties of the BRAF- and CRAF-CRDs and found that the BRAF-CRD was a stronger mediator of PS binding and autoinhibition, and that exchanging the BRAF-CRD with that of CRAF was sufficient to activate the transforming potential of BRAF. These findings suggest that the enhanced autoinhibitory activity of the BRAF-CRD may be required to maintain BRAF in a quiescent state, as BRAF has the highest basal catalytic activity of all the RAF kinases, due largely to the constitutive negative charge of the BRAF N-region sequences[40, 41]. In support of this model, CRAF proteins containing the BRAF N-region exhibited increased catalytic activity and were weakly transforming, consistent with the reduced autoinhibitory activity of the CRAF-CRD. Moreover, while incorporation of mutations analogous to the BRAF RASopathy-associated T241P, Q257R or Q262K into the CRAF-CRD was not sufficient to promote focus formation, their incorporation into CRAF hybrid proteins containing the BRAF N-region resulted in mutant proteins that had significant transforming activity. Thus, the high basal catalytic activity of BRAF combined with the critical autoinhibitory function of the BRAF-CRD may account for why the BRAF-CRD is a mutational hotspot in the RASopathies, whereas no CRD mutations in CRAF have been reported.

In conclusion, analysis of the RASopathy BRAF-CRD mutations has provided significant insight regarding the relative importance of the distinct activities of the BRAF-CRD and has revealed functional differences between RAF family members that are relevant to human disease (Fig. 7c). Importantly, the critical role for autoinhibition in BRAF regulation suggests that stabilizing the autoinhibited state using pharmacological approaches may have therapeutic benefit in preventing the aberrant activation of BRAF that frequently occurs in human cancer and the RASopathies. Moreover, the NanoBRET autoinhibition assay developed in this study could prove highly useful in the identification of such novel therapeutic compounds.

ACKNOWLEDGMENTS

We thank John-Paul Denson, Matt Drew, Dominic Esposito, Bill Gillette, Jose Sanchez Hernandez, Shelley Perkins, Nitya Ramakrishnan, Kelly Snead, Troy Taylor, and Vanessa Wall (FNLCR Protein Expression Laboratory) for the production and characterization of the isolated CRD proteins for SPR analysis and Linda Miller (LCDS) for technical support. This project has been funded in

whole or in part with Federal funds from the National Cancer Institute, National Institutes of Health, under project number ZIA BC 010329 (D.K.M) and Contract No. HHSN261200800001E (A.G.S.).

AUTHOR CONTRIBUTIONS

R.S.-S. and D.K.M. conceived the project, designed the experiments, and interpreted the data with contributions from A.G.S. R.S.-S. developed the NanoBRET assay to quantify RAF autoinhibitory interactions, conducted all autoinhibition assays, and performed the cell imaging studies; E.M.T. generated critical reagents and conducted the BRET RAS-RAF interaction assays; E.M.T., D.A.R., and R.S.-S. performed the focus forming assays; C.A. and M.E.W. conducted the surface plasmon resonance analysis; and C.I and J.S performed the zebrafish experiments. R.S.S. and D.K.M. wrote the manuscript.

DECLARATION OF INTERESTS

The authors declare no competing interests.

METHODS

Cell lines and culture conditions. HEK293FT, Phoenix-Eco, NIH 3T3, and COS-7 cells were cultured in DMEM supplemented with 10% fetal bovine serum (FBS), 2 mM L-glutamine, and 1% penicillin/streptomycin. All cells were cultured at 37ºC with 5% CO_2.

RAF CRD protein production. Wild type and mutant human BRAF (232-284) and CRAF/RAF1 (136-188): Entry clones were synthesized with an upstream tobacco etch virus (TEV) protease cleavage site (ENLYFQ/G) and optimized for expression in E. coli by ATUM (Newark, CA). Entry clone inserts were transferred by Gateway recombinational cloning (ThermoFisher, Carlsbad, CA) to pDest-566 (Addgene #11517), a T7-based E. coli expression vector encoding an N-terminal His6-MBP (maltose-binding protein) fusion. All CRD proteins were expressed using LB medium supplemented with 300 mM $ZnCl_2$ as outlined for CRAF (52-188) in [42]. For 2-liter working volume fermentations, 3-liter Bioflo 110 (Eppendorf) were used, and 20-liter Bioflo IV (Eppendorf) were used for 15-liter working volumes. Antifoam 204 (Sigma) was added at 0.075% v/v and 0.017% v/v, respectively, to the 2- and 15-liter fermenters. All proteins were purified essentially as outlined

in [43] for CRAF RBD (52-131). Specifically, 5 mM TCEP was used in all buffers and the protein occasionally eluted overlapping the salt peak during SEC which then required an additional dialysis step (3K MWCO) to the final buffer.

SPR measurements. SPR binding experiments were collected on a Biacore T200 Instrument (GE Healthcare). Anti-His6 monoclonal antibody (Abcam) was amine coupled to the carboxy-methylated dextran surface of a CM5 sensor chip (GE Healthcare) using standard amine coupling chemistry. The CM5 chip surface was first activated with 0.1 M N-hydroxysuccinimide and 0.4 M N-ethyl-N'-(3-dimethylaminopropyl) carbodimide at a flow rate of 20 µl/min. Next, anti-His6 monoclonal antibody was diluted to 20 µg/ml in 10 mM sodium acetate (pH 5.0) and injected on all 4 flow cells until a density of approximately 10000 Response Units (RU) was attached. His6-tagged MSP1D1 nanodiscs composed of either 1-palmitoyl-2-oleoyl-glycero-3-phosphocholine (POPC) or 80:20 1-palmitoyl-2-oleoyl-glycero-3-phosphocholine:1-palmitoyl-2-oleoyl-glycero-3-phosphoL-serine (POPC:POPS) were prepared as described previously[44]. Nanodiscs were captured (2000-4000 RU) on flow cells 2 and 4 containing the anti-His6 antibody surfaces. Flow cells 1 and 4 were used for referencing and a series of buffer injections were added to establish a stable baseline. BRAF- or CRAF-CRD proteins were diluted in 2-fold from 5 – 0.31 µM in a buffer composed of 20 mM Hepes pH 7.0, 150 mM NaCl and injected over all the flow cells at 30 µl/min. SPR sensorgrams were normalized by the capture level of nanodiscs to allow direct comparison between different experimental runs. Equilibrium binding constants (K_d) were calculated using Prism. Complementary experiments were performed using captured liposomes as described previously[37]. Specifically, L1 chips were activated with two injections of 20 mM CHAPS followed by liposomes (5 mM) composed of POPC or 80:20 POPC:POPS on flow cells 2 and 4 (capture levels 3500 – 5000). Flow cells 1 and 3 were used for referencing purposes. Following liposome capture a series of buffer injections (20 mM Hepes pH 7.0, 150 mM NaCl) were performed to obtain a stable baseline. BRAF-CRD proteins were diluted 2-fold from 15 – 0.12 µM in buffer and consecutively injected onto the captured liposomes. The L1 was regenerated using two injections of 20 mM CHAPS. The data was analyzed to calculate the equilibrium partition coefficient (K_p) according to Figueira et al[45].

Transfection and lysis of cells. All cell lines were plated at ~70% confluency 16-20 hours prior to transfection. Cells were then transfected using the XtremeGENE9 transfection reagent per the manufacturer's instructions, with a 2:1 ratio of XtremeGENE9 to DNA. For lysis, cells were washed twice with ice cold PBS and lysed in NP40 buffer (20mM Tris [pH 8.0], 137 mM NaCl, 10% glycerol, 1% NP-40 alternative, 0.15 U/mL aprotinin, 1 mM phenylmethylsulfonyl fluoride, 0.5 mM sodium vanadate, 20 mM leupeptin) at 4°C for 15 minutes on a rocking platform. Lysates were clarified by centrifugation at 14,000 rpm for 10 min at 4°C, following which the protein content was determined by Bradford assays.

NanoBRET autoinhibition assay. HEK-293FT cells were seeded into 6-well tissue culture plates at a concentration of $4x10^5$ cells/well. 16 hours after plating, cells were co-transfected using 5 ng of the indicated NanoLuc-$CRAF^{CAT}$ construct and 20 ng of the indicated Halo-$BRAF^{REG}$ construct (per well). Twenty-four hours later, cells were collected and resuspended in serum-free/phenol free Opti-MEM (Gibco). 1 µl/ml HaloTag NanoBRET 618 ligand was added to the cell suspension and cells were seeded at a concentration of 8 $x10^3$ cells per well of a 384-well plate in quadruplicate (BioTek, Winooski, VT), with the remaining cells plated into a fresh 6-well tissue culture plate. After 24 hours, 10 µl/ml NanoBRET NanoGlo substrate was added to each well of cells to be monitored for NanoBRET, and donor (460nm) and acceptor (618nm) emissions were measured using a Perkins Elmer Envision plate reader (#2104-0010A containing a 460nm/50nm emission filter and a 610nm LP filter). Cells seeded into the 6-well plates were lysed and examined by immunoblot analysis using antibodies recognizing the Halo-tag for RAF^{REG} detection and the NanoLuc tag for RAF^{CAT} detection to ensure equal expression levels across conditions.

BRET RAS-RAF interaction assay. HEK293FT cells were seeded into 12-well dishes at a concentration of 1x105 cells/well. 16 hours after plating, pCMV5-Venus-KRAS4B and pLHCX-CMV-Raf-Rluc8 constructs[30] were transfected into cells using a calcium phosphate protocol. Duplicate 12-point saturation curves were generated in which the concentration of the energy donor construct (Rluc8) was held constant (62.5 ng) as the concentration of the energy acceptor plasmid (Venus) increased (0-1.0 µg). 48 hours after transfection, cells from each well were collected, washed, and resuspended in PBS (500 µL). 30 µL of the cell suspension was plated in duplicate into wells of a 384-well white-walled plate (PerkinElmer CulturePlate) and coelenterazine-h was

added to a final concentration of 3.375 μM. The BRET and Rluc8 emissions were measured simultaneously using a PHERAstar Plus plate reader (BMG Labtech), with BRET monitored at 535 nm (bandwidth 30 nm) and Rluc8 measured at 475 nm (bandwidth 30 nm). To monitor the increasing levels of acceptor expression, 90 μL of the cell suspension was also plated in duplicate into wells of a 96-well black-walled plate (PerkinElmer OptiPlate), and Venus fluorescence was determined using an excitation wavelength of 485 nm (5 nm bandwidth) and fluorescence read at 530 nm (5 nm bandwidth) using a Tecan Infinite M1000 plate reader. The BRET ratio was determined by calculating the 535/475 ratio for a given sample (sample BRET) and was normalized to the BRET signal from cells expressing the donor construct alone to enable comparisons between experiments. The normalized mBRET signal was calculated as follows: (1000 X (sample BRET ratio/background BRET ratio)) – 1000. The acceptor/donor ratio (Venus emission/Rluc8 emission) for each data point was background corrected and equalized against a control where equal quantities of the Venus (acceptor) and Rluc8 (donor) constructs were transfected to allow for comparisons between experiments. Data was analyzed using GraphPad Prism. Non-linear regression was used to plot the best fit hyperbolic curve, and values for $BRET_{max}$ and $BRET_{50}$ were obtained from the calculated best fit curves.

Focus forming assay. Recombinant retroviruses expressing the BRAF proteins of interest were generated by transfecting a 100 mm tissue culture dish of Phoenix-Eco cells with 6 μg of DNA construct using the XtremeGENE9 protocol described above. Viral supernatants were collected 48 hours post-transfection, centrifuged twice at 1500 rpm for 10 minutes, and either stored at -80°C or used directly. NIH-3T3 cells were plated into 60 mm tissue culture dishes at a concentration of 2 x 10^5 cells/dish. After 16 hours, cells were infected with the indicated recombinant retrovirus in media containing 4% FBS and 8 μg/mL polybrene. 24 hours later, cells were trypsinized and plated into two 100 mm dishes, one of which contained 5 μg/mL puromycin. After 2-4 weeks of culture, cells were fixed with 3.7% formaldehyde and stained with 1% methylene blue.

Zebrafish embryo injections and analysis. Fish care and animal work was approved by the National Cancer Institute at Frederick Animal Care and Use committee (Study Proposal 17-416). All capped mRNAs were generated from NotI linearized pCS2+ vector templates using the mMESSAGE mMACHINE T3 kit (ThermoFisher Scientific). AB-Tübingen zebrafish embryos

were microinjected at the one cell stage with 66 pg/nL of mRNA encoding either WT or mutant FLAG-BRAF proteins or WT or mutant BRAF-Venus fusion proteins. After injection, embryos were maintained at 25°C until analysis. For convergence-extension cell movement assays (CE assays), embryos at the 3-6 somite stage were embedded oriented laterally in 1% low-melt agarose (Invitrogen, Carlsbad, CA) and imaged under bright field (to determine yolk elongation by taking major and minor axis measurements) and under fluorescent conditions (to monitor expression of the BRAF-Venus proteins). Larvae collected three days post-fertilization (dpf) were positioned laterally and imaged under bright field to monitor for pericardial edema. For ceratohyal (CH) angle and length measurements, Tg (*col2a1aBAC:GFP*) embryos were injected with 33 pg/nL RNA and treated with 0.003% 1-phenyl 2-thiourea to block pigmentation. At 5dpf, larvae were anesthetized with 0.2 mg/mL Tricaine in E3 and positioned dorsally against the side of grooves made by a mold (World Precision Instruments) in 1% low-melt agarose.

Images under bright field condition were taken using a 2X water immersion objective (0.06 NA) for CE assays, and image acquisition (~ 200 µm z-stacks with 5 µm step size) of Venus fluorescence was performed using a 10X objective (0.3 NA) for CH analyses. The Nikon Eclipse Ni-E upright microscope was equipped with a DS-Ri2 camera. All measurements were performed using the Nikon NIS Elements Analysis software and processing of images were carried out using ImageJ and Photoshop. Statistical analyses were conducted using GraphPad Prism

Cell imaging. COS-7 cells ($5x10^4$) were plated onto 35 mm glass-bottom dishes (MATEK) that had been pre-coated with 10 µg/ml human placental type IV collagen. 16 hours after plating, cells were transfected with the indicated DNA constructs, incubated for 24 hours at 37°C under 5% CO_2, and then serum starved overnight. The following day, cells were washed twice with PBS, fixed for 10 minutes in 4% paraformaldehyde, washed twice again with PBS, and then imaged using a 63x oil objective on a Zeiss LSM710 confocal microscope.

RAF kinase assay. Cells expressing the indicated FLAG-RAF proteins were lysed under stringent conditions in RIPA buffer to disrupt protein complexes. The Raf proteins were immunopurified and incubated in kinase buffer (30 mM Tris pH 7.4, 10 mM $MnCl_2$, 5 mM $MgCl_2$, 1 mM DTT, 16.5 µM ATP) containing 20 µCi [γ-32P]ATP and kinase-inactive MEK. Samples were resolved by SDS-

PAGE, and after transfer to nitrocellulose, the amount of radioactivity incorporated into MEK was determined by scintillation counting. RAF activity levels were normalized to Raf protein levels.

Antibodies and reagents. BRAF (H-145) rabbit polyclonal, Santa Cruz Biotechnology cat# sc-9002; RRID:AB_2067494; HaloTag mouse monoclonal, Promega cat# G9211, RRID:AB_2688011; NanoLuc (Nluc) luciferase antibody, R&D Systems cat# MAB100261; FLAG M2 antibody, Millipore/Sigma cat# F3165, RRID:AB_439685; FLAG (L5) rat monoclonal, BioLegend cat# 637304, RRID:AB_1134267; MEK1 mouse monoclonal, BD Biosciences cat# 61022, RRID:AB_397528; pS217/221-MEK rabbit polyclonal, Cell Signaling Technology cat# 9121, RRID:AB_331648; α-Tubulin mouse monoclonal, Millipore Sigma cat# T6199; RRID:AB_477583.

REFERENCES

1. Lavoie, H. & Therrien, M. Regulation of RAF protein kinases in ERK signalling. *Nat Rev Mol Cell Biol* **16**, 281-298 (2015).
2. Terrell, E.M. & Morrison, D.K. Ras-Mediated Activation of the Raf Family Kinases. *Cold Spring Harbor perspectives in medicine* **9** (2019).
3. Nan, X. *et al.* Single-molecule superresolution imaging allows quantitative analysis of RAF multimer formation and signaling. *Proc Natl Acad Sci U S A* **110**, 18519-18524 (2013).
4. Park, E. *et al.* Architecture of autoinhibited and active BRAF-MEK1-14-3-3 complexes. *Nature* (2019).
5. Freeman, A.K., Ritt, D.A. & Morrison, D.K. Effects of Raf dimerization and its inhibition on normal and disease-associated Raf signaling. *Mol Cell* **49**, 751-758 (2013).
6. Hu, J. *et al.* Allosteric activation of functionally asymmetric RAF kinase dimers. *Cell* **154**, 1036-1046 (2013).
7. Dougherty, M.K. *et al.* Regulation of Raf-1 by direct feedback phosphorylation. *Mol Cell* **17**, 215-224 (2005).
8. Ritt, D.A., Monson, D.M., Specht, S.I. & Morrison, D.K. Impact of feedback phosphorylation and Raf heterodimerization on normal and mutant B-Raf signaling. *Mol Cell Biol* **30**, 806-819 (2010).
9. Schubbert, S., Shannon, K. & Bollag, G. Hyperactive Ras in developmental disorders and cancer. *Nat Rev Cancer* **7**, 295-308 (2007).
10. Rauen, K.A. The RASopathies. *Annu Rev Genom Hum G* **14**, 355-369 (2013).
11. Tidyman, W.E. & Rauen, K.A. Pathogenetics of the RASopathies. *Human molecular genetics* **25**, R123-R132 (2016).
12. Pandit, B. *et al.* Gain-of-function RAF1 mutations cause Noonan and LEOPARD syndromes with hypertrophic cardiomyopathy. *Nat Genet* **39**, 1007-1012 (2007).
13. Razzaque, M.A. *et al.* Germline gain-of-function mutations in RAF1 cause Noonan syndrome. *Nature Genetics* **39**, 1013-1017 (2007).

14. Niihori, T. *et al.* Germline KRAS and BRAF mutations in cardio-facio-cutaneous syndrome. *Nat Genet* **38**, 294-296 (2006).
15. Rodriguez-Viciana, P. *et al.* Germline mutations in genes within the MAPK pathway cause cardio-facio-cutaneous syndrome. *Science (New York, N.Y.)* **311**, 1287-1290 (2006).
16. Roy, S., Lane, A., Yan, J., McPherson, R. & Hancock, J.F. Activity of plasma membrane-recruited Raf-1 is regulated by Ras via the Raf zinc finger. *J Biol Chem* **272**, 20139-20145 (1997).
17. Bondeva, T., Balla, A., Varnai, P. & Balla, T. Structural determinants of Ras-Raf interaction analyzed in live cells. *Molecular Biology of the Cell* **13**, 2323-2333 (2002).
18. Ghosh, S., Strum, J.C., Sciorra, V.A., Daniel, L. & Bell, R.M. Raf-1 kinase possesses distinct binding domains for phosphatidylserine and phosphatidic acid. Phosphatidic acid regulates the translocation of Raf-1 in 12-O-tetradecanoylphorbol-13-acetate-stimulated Madin-Darby canine kidney cells. *J Biol Chem* **271**, 8472-8480 (1996).
19. Ghosh, S. *et al.* The cysteine-rich region of raf-1 kinase contains zinc, translocates to liposomes, and is adjacent to a segment that binds GTP-ras. *J Biol Chem* **269**, 10000-10007 (1994).
20. Hekman, M. *et al.* Associations of B- and C-Raf with cholesterol, phosphatidylserine, and lipid second messengers. *J. Biol. Chem.* **277**, 24090-24102 (2002).
21. Ghosh, S. & Bell, R.M. Identification of discrete segments of human Raf-1 kinase critical for high affinity binding to Ha-Ras. *J Biol Chem* **269**, 30785-30788 (1994).
22. Hu, C.D. *et al.* Cysteine-rich region of Raf-1 interacts with activator domain of post-translationally modified Ha-Ras. *J Biol Chem* **270**, 30274-30277 (1995).
23. Brtva, T.R. *et al.* Two distinct Raf domains mediate interaction with Ras. *J Biol Chem* **270**, 9809-9812 (1995).
24. Fang, Z. *et al.* Multivalent assembly of KRAS with the RAS-binding and cysteine-rich domains of CRAF on the membrane. *Proc Natl Acad Sci U S A* (2020).
25. Tran, T.H. *et al.* KRAS interaction with RAF1 RAS-binding domain and cysteine-rich domain provides insights into RAS-mediated RAF activation. *Nature communications* **12**, 1176 (2021).
26. Chong, H. & Guan, K.-L. Regulation of Raf through phosphorylation and N-terminus-C terminus interaction. *J. Biol. Chem.* **278**, 36269-36276 (2003).
27. Cutler, R.E., Jr., Stephens, R.M., Saracino, M.R. & Morrison, D.K. Autoregulation of the Raf-1 serine/threonine kinase. *Proc Natl Acad Sci U S A* **95**, 9214-9219 (1998).
28. Tran, N.H., Wu, X. & Frost, J.A. B-Raf and Raf-1 are regulated by distinct autoregulatory mechanisms. *J Biol Chem* **280**, 16244-16253 (2005).
29. Machleidt, T. *et al.* NanoBRET--A Novel BRET Platform for the Analysis of Protein-Protein Interactions. *ACS Chem Biol* **10**, 1797-1804 (2015).
30. Terrell, E.M. *et al.* Distinct Binding Preferences between Ras and Raf Family Members and the Impact on Oncogenic Ras Signaling. *Mol Cell* **76**, 872-884 e875 (2019).
31. Patterson, V.L. & Burdine, R.D. Swimming toward solutions: Using fish and frogs as models for understanding RASopathies. *Birth Defects Res* **112**, 749-765 (2020).
32. Jindal, G.A. *et al.* In vivo severity ranking of Ras pathway mutations associated with developmental disorders. *Proc Natl Acad Sci U S A* **114**, 510-515 (2017).
33. Askary, A. *et al.* Iroquois Proteins Promote Skeletal Joint Formation by Maintaining Chondrocytes in an Immature State. *Dev Cell* **35**, 358-365 (2015).

34. Sarkozy, A. *et al.* Germline BRAF mutations in Noonan, LEOPARD, and cardiofaciocutaneous syndromes: molecular diversity and associated phenotypic spectrum. *Hum Mutat* **30**, 695-702 (2009).
35. Winkler, D.G. *et al.* Identification of residues in the cysteine-rich domain of Raf-1 that control Ras binding and Raf-1 activity. *J Biol Chem* **273**, 21578-21584 (1998).
36. Improta-Brears, T., Ghosh, S. & Bell, R.M. Mutational analysis of Raf-1 cysteine rich domain: requirement for a cluster of basic aminoacids for interaction with phosphatidylserine. *Mol Cell Biochem* **198**, 171-178 (1999).
37. Travers, T. *et al.* Molecular recognition of RAS/RAF complex at the membrane: Role of RAF cysteine-rich domain. *Sci Rep* **8**, 8461 (2018).
38. Oancea, E., Teruel, M.N., Quest, A.F. & Meyer, T. Green fluorescent protein (GFP)-tagged cysteine-rich domains from protein kinase C as fluorescent indicators for diacylglycerol signaling in living cells. *J Cell Biol* **140**, 485-498 (1998).
39. Verbeek, D.S., Goedhart, J., Bruinsma, L., Sinke, R.J. & Reits, E.A. PKC gamma mutations in spinocerebellar ataxia type 14 affect C1 domain accessibility and kinase activity leading to aberrant MAPK signaling. *J Cell Sci* **121**, 2339-2349 (2008).
40. Marais, R., Light, Y., Paterson, H.F., Mason, C.S. & Marshall, C.J. Differential regulation of Raf-1, A-Raf, and B-Raf by oncogenic ras and tyrosine kinases. *J Biol Chem* **272**, 4378-4383 (1997).
41. Emuss, V., Garnett, M., Mason, C. & Marais, R. Mutations of C-RAF are rare in human cancer because C-RAF has a low basal kinase activity compared with B-RAF. *Cancer research* **65**, 9719-9726 (2005).
42. Lakshman, B. *et al.* Quantitative biophysical analysis defines key components modulating recruitment of the GTPase KRAS to the plasma membrane. *J Biol Chem* **294**, 2193-2207 (2019).
43. Kopra, K. *et al.* Homogeneous Dual-Parametric-Coupled Assay for Simultaneous Nucleotide Exchange and KRAS/RAF-RBD Interaction Monitoring. *Anal Chem* **92**, 4971-4979 (2020).
44. Agamasu, C. *et al.* KRAS Prenylation Is Required for Bivalent Binding with Calmodulin in a Nucleotide-Independent Manner. *Biophys J* **116**, 1049-1063 (2019).
45. Figueira, T.N. *et al.* Quantitative analysis of molecular partition towards lipid membranes using surface plasmon resonance. *Sci Rep* **7**, 45647 (2017).

Figure Legends

Fig 1. Identification of RASopathy-associated BRAF-CRD mutations that modulate PS binding. **a** The amino acid sequence of the BRAF-CRD is shown with arrows indicating the RASopathy-associated CRD mutations (left panel). A pie chart is also shown depicting the percent occurrence of a particular mutation in the BRAF-CRD (right panel). Data was collected from nseuronet.com. **b** A 2-fold dilution series of purified 5μM WT or mutant BRAF-CRD proteins was injected over nanodiscs containing 20% POPS/80% POPC or 100% POPC, and binding responses were determined by SPR. Sensorgrams were normalized to the WT-BRAF-CRD binding response. **c** Binding slopes of the CRD mutants were normalized to the binding slope of the WT-CRD (with WT equaling 1), and the graph represents the mean of two independent experiments ± SD. **d** The partitioning coefficients for binding of WT and mutant BRAF-CRDs to liposomes containing 20% POPS/80% POPC was determined, and the graph represents the mean of three independent experiments ± SD. Student's *t*-test (two- tailed, assuming unequal variance) was performed comparing WT-BRAF and each of the CRD mutants. ns, not significant; *, $P < 0.05$, P **, $P < 0.01$; ***, $P < 0.001$, and ****, $P < 0.0001$. **e**,**f** Serum-starved COS-7 cells transiently expressing the indicated GFP-CRD proteins were examined immunoblot analysis to evaluate GFP-CRD levels (**e**) and by confocal microscopy to determine the subcellular localization of the isolated CRD proteins (**f**). A tracing depicting the GFP intensity in the area indicated by the yellow line is also shown. The images are representative of two independent experiments with similar results.

Fig 2. Identification of RASopathy-associated BRAF-CRD mutations that disrupt RAF autoinhibitory interactions. **a** NanoBRET interaction assay showing the BRET signal generated when increasing amounts of the WT-BRAF^{REG}-Halo construct were co-transfected with a constant amount Nano-WT-BRAF^{CAT}. Data represent the mean of BRET signals from quadruplicate wells ± SD and are representative of three independent experiments. **b** Lysates of 293FT cells transiently expressing Nano-WT-BRAF^{CAT} alone or co-expressing Nano-WT-BRAF^{CAT} with increasing amounts of WT-BRAF^{REG}-Halo were examined by immunoblot analysis for WT-BRAF^{REG}-Halo, Nano-WT-BRAF^{CAT}, and pMEK levels. Normalized pMEK levels were determined. Blots are representative of three independent experiments with similar results. **c** NanoBRET assay measuring

the interaction of WT- or mutant $BRAF^{REG}$-Halo proteins and Nano-WT-$BRAF^{CAT}$. Also shown, is the effect of co-expressing HA-tagged $KRAS^{G12V}$ with the WT BRET pair and the effect of co-expressing V600E-$BRAF^{CAT}$ with WT-$BRAF^{REG}$. Data points represent BRET signals (normalized to WT set at 100) of quadruplicate wells from 3 independent experiments ± SD. Student's *t*-test (two- tailed, assuming unequal variance) was performed comparing WT-BRAF and each of the CRD mutants. ns, not significant and ****, $P < 0.0001$. Cell lysates were also examined by immunoblot analysis for $BRAF^{REG}$-Halo (REG), Nano-$BRAF^{CAT}$ (CAT), and HA-KRAS levels. **d** Cryo-EM structure of autoinhibited BRAF, showing the CRD (magenta) contacting both the Raf catalytic domain (blue) and a bound dimer of 14-3-3 (yellow/gold). CRD residues mutated in the RASopathies are annotated and their side chains shown (PDB: 6NYB).

Fig 3. Effect of RASopathy-associated BRAF-CRD mutations on RAS-RAF binding and BRAF signaling activity. **a** BRET saturation curves are shown examining the interaction of WT or mutant $BRAF^{FL}$-RLuc8 proteins with Venus-$KRAS^{G12V}$. **b** $BRET_{max}$ and $BRET_{50}$ values derived from the saturation curves shown in **a** are listed ± standard error. Of note, expression levels of the donor and acceptor constructs were monitored and are incorporated into the calculations determining the $BRET_{max}$ and $BRET_{50}$ values as described in the methods. Saturation curves were repeated 3 times with similar results. **c** Lysates of serum-starved NIH-3T3 cells expressing the indicated FLAG-$BRAF^{FL}$ proteins were examined for pMEK, FLAG-$BRAF^{FL}$, and total MEK levels. Normalized pMEK levels were determined. Blots are representative of 3 independent experiments with similar results. **d** NIH-3T3 cells were infected with retroviruses encoding the indicated WT or mutant FLAG-$BRAF^{FL}$ proteins. Three weeks post-infection, foci were visualized by methylene blue staining. Focus forming assays were repeated at least 3 times with similar results. Quantification of foci number is cited in Supplementary Table 2.

Fig 4. Expression of RASopathy-associated BRAF-CRD mutants induces alterations in zebrafish embryos. **a** mRNA encoding the indicated Venus-tagged BRAF proteins were injected into one-cell stage zebrafish embryos and the embryos were measured at 11 hrs post fertilization (hpf) to determine the major to minor axis ratio. Shown are representative images of the embryos

and the expression levels of the BRAF-Venus proteins (left). The average axis ratio of embryos analyzed in three independent experiments is shown ± SEM (right). Average axis ratio of unjected embryos is 1 ± SEM 0.005. **b** mRNA encoding the indicated BRAF proteins were injected into one-cell stage zebrafish embryos and the embryos were examined 3 days post fertilization (dpf) for heart edema. Zebrafish embryos with normal and edemic hearts are shown (left). The graph represents the percentage of embryos with heart edema in three independent experiments ± SEM (right). **c** Embryos from the *Tg (col2a1aBAC:GFP)* transgenic line were injected at the one-cell stage with mRNAs encoding the indicated BRAF proteins. The ceratohyal is marked by GFP in the transgenic embryos at 5 dpf and the angle in the ceratohyal (dotted red line) was determined. Representative images are shown (left). The graph represents the quantification of the angle of the ceratohyal from four independent experiments ± SEM. Average ceratohyal angle for uninjected embryos is 59° ± SEM 3.0 **d** Summary of phenotypic characteristics of RASopathy patients with BRAF-CRD mutations. Data was collected from nseuronet.com and references are cited in Supplementary Table 3. For statistical analysis (a-c), one-way analysis of variance (ANOVA) with Bonferroni correction was used . ns, not significant; *, $P < 0.05$, P **, $P < 0.01$; ***, $P < 0.001$, and ****, $P < 0.0001$.

Fig. 5. The CRDs of BRAF and CRAF differ in their abilities to bind PS. **a** The indicated BRAF- and CRAF-CRD proteins were examined by SPR for binding to nanodiscs containing 20% POPS/80% POPC. Sensorgrams were normalized to the WT-BRAF-CRD binding response. **b**, Binding slopes for the CRAF-CRD and the indicated CRD mutants were normalized to the binding slope of the BRAF-CRD (with BRAF-CRD equaling 1), and the graph represents the mean of two independent experiments ± SD. Student's *t*-test (two- tailed, assuming unequal variance) was performed. ns, not significant and ***, $P < 0.001$. **c** Serum-starved COS-7 cells transiently expressing the indicated GFP-CRD proteins were examined by confocal microscopy to determine the subcellular localization of the isolated CRD proteins. A tracing depicting the GFP intensity in the area indicated by the yellow line is shown below the images. Cell lysates were also examined by immunoblot analysis for GFP-CRD levels, with α-tubulin used as a protein loading control. The images are representative of two independent experiments with similar results. **d** Electrostatic

surface representation of the BRAF-CRD (PDB: 6NYB) and the CRAF-CRD (PDB: 1FAR) are shown, with blue and red representing positively and negatively charged areas, respectively. Shown is a top view of the membrane binding interface of the CRDs with key residues indicated. **e** Electrostatic surface charge distribution of the BRAF-CRD (PDB: 6NYB) is shown, with the RASopathy-associated PC mutations indicated.

Fig. 6. The CRDs of BRAF and CRAF differ in their abilities to mediate autoinhibition. **a** NanoBRET interaction assay showing the BRET signal generated when WT- $BRAF^{REG}$, C-CRD-$BRAF^{REG}$, WT-$CRAF^{REG}$, or B-CRD-$CRAF^{REG}$-Halo were co-transfected with Nano-WT-$BRAF^{CAT}$ (left) or Nano-WT-$CRAF^{CAT}$ (right). Cell lysates were also examined by immunoblot analysis for RAF^{REG} and RAF^{CAT} proteins levels. Data points represent quadruplicate wells from 2 independent experiments ± SD. **b** BRET saturation curves are shown examining the interaction of WT or C-CRD-$BRAF^{FL}$-RLuc8 proteins with Venus-$KRAS^{G12V}$. $BRET_{max}$ and $BRET_{50}$ values are listed ± standard error. Saturation curves were repeated at least 2 times with similar results. **c** NIH-3T3 cells were infected with retroviruses encoding the indicated FLAG-$BRAF^{FL}$ variants. Three weeks post-infection, foci were visualized by methylene blue staining. Focus forming assays were repeated 2 times with similar results. Quantification of foci number is cited in Supplementary Table 2. **d** NanoBRET assay measuring the interaction of WT- or mutant $BRAF^{REG}$-Halo proteins and Nano-WT-$BRAF^{CAT}$. Cell lysates were also examined by immunoblot analysis for $BRAF^{REG}$ and $BRAF^{CAT}$ proteins levels. Data points represent quadruplicate wells from 2 independent experiments ± SD. Proximity of the BRAF-CRD residue T244 (magenta) and the BRAF catalytic domain residue R719 (blue) is also shown. (PDB: 6NYB). For **a**, **d**, student's *t*-test (two- tailed, assuming unequal variance) was performed. ns, not significant and ****, $P < 0.0001$.

Fig. 7. Analysis of CRAF proteins containing mutations analogous to the RASopathy BRAF-CRD mutations. **a** NIH-3T3 cells were infected with retroviruses encoding the indicated WT or mutant FLAG- $CRAF^{FL}$ proteins. Three weeks post-infection, foci were visualized by methylene blue staining. Focus forming assays were repeated three times with similar results. Quantification of foci number is cited in Supplementary Table 2. **b** In vitro kinase assays were performed to

demonstrate the increased catalytic activity of FLAG-CRAF^{FL} containing the N-region sequence of BRAF (N-region swap) versus WT-FLAG-CRAF^{FL} (with WT activity equaling 1). Data represent the mean of duplicate assays in 3 independent experiments ± SD. . Student's *t*-test (two- tailed, assuming unequal variance) was performed. ****, $P < 0.0001$. **c** Model comparing the properties of the BRAF- and CRAF-CRDs. See text for details.

DECLARATION OF INTERESTS

The authors declare no competing interests

Figure 1

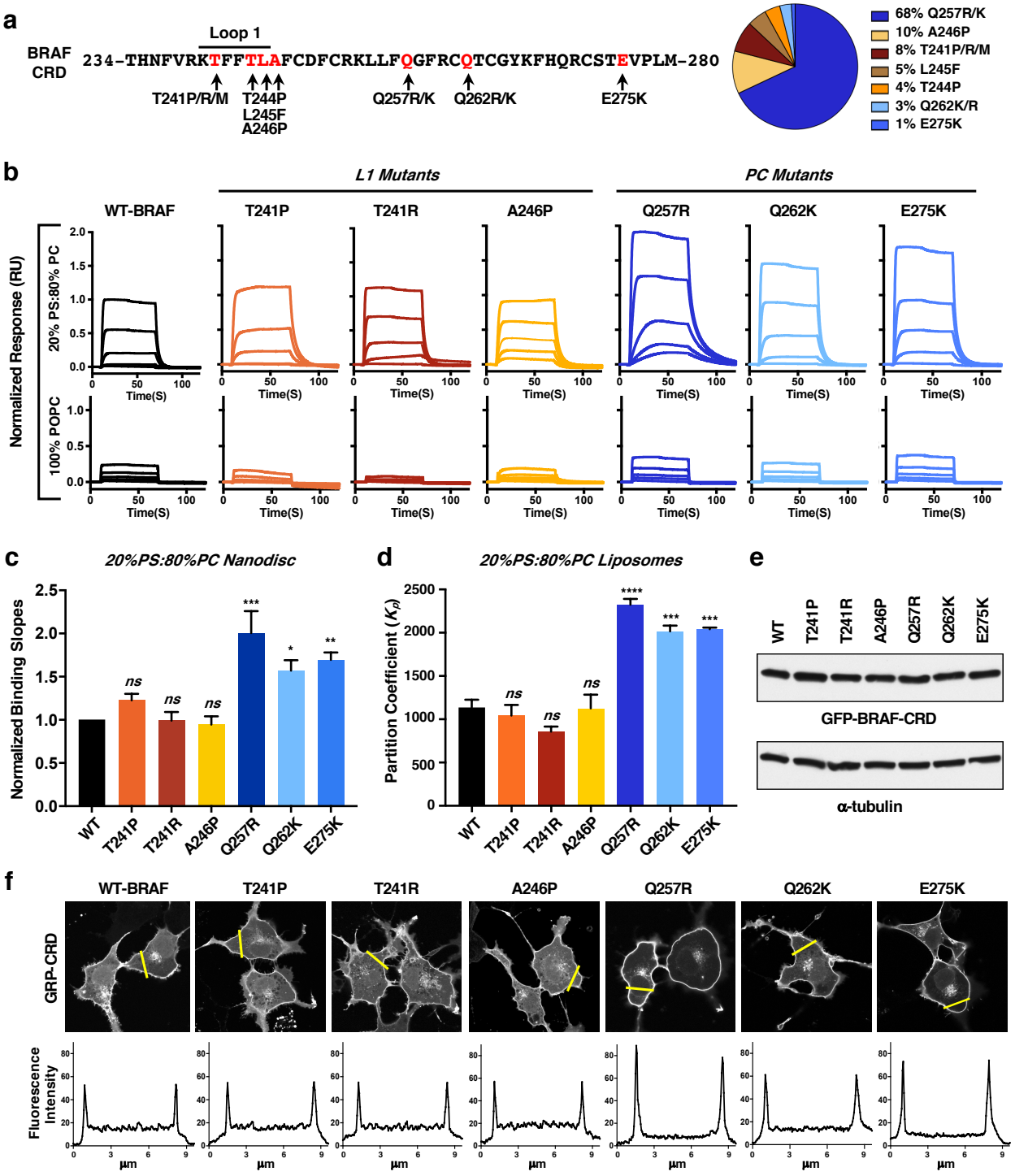
a
Loop 1
BRAF CRD
234-THNFVRKTFFTLAFCDFCRKLLFQGFRCQTCGYKFHQRCSTEVPLM-280
T241P/R/M
T244P
L245F
A246P
Q257R/K
Q262R/K
E275K
68% Q257R/K
10% A246P
8% T241P/R/M
5% L245F
4% T244P
3% Q262K/R
1% E275K
b
L1 Mutants
PC Mutants
WT-BRAF
T241P
T241R
A246P
Q257R
Q262K
E275K
Normalized Response (RU)
20% PS:80% PC
100% POPC
Time(S)
c
20%PS:80%PC Nanodisc
Normalized Binding Slopes
ns
***
*
**
WT
T241P
T241R
A246P
Q257R
Q262K
E275K
d
20%PS:80%PC Liposomes
Partition Coefficient (Kp)
****
e
GFP-BRAF-CRD
α-tubulin
f
GRP-CRD
Fluorescence Intensity
µm

Figure 2

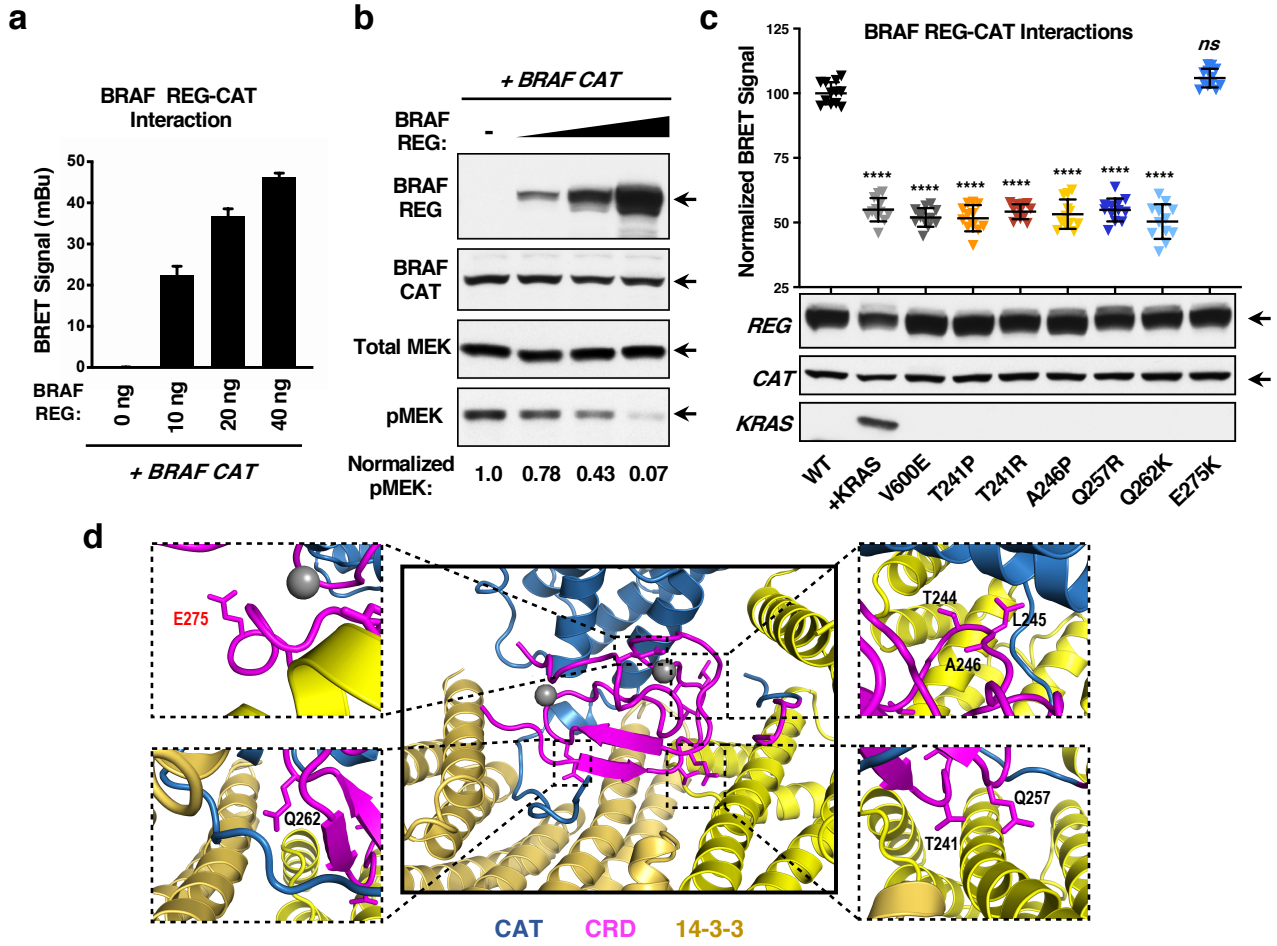
a
BRAF REG-CAT Interaction
BRET Signal (mBu)
50
40
30
20
10
0
BRAF REG:
0 ng
10 ng
20 ng
40 ng
+ BRAF CAT
b
+ BRAF CAT
BRAF REG:
-
BRAF REG
BRAF CAT
Total MEK
pMEK
Normalized pMEK:
1.0
0.78
0.43
0.07
c
BRAF REG-CAT Interactions
Normalized BRET Signal
125
100
75
50
25
ns
****
REG
CAT
KRAS
WT
+KRAS
V600E
T241P
T241R
A246P
Q257R
Q262K
E275K
d
E275
T244
L245
A246
Q262
Q257
T241
CAT
CRD
14-3-3

Figure 3

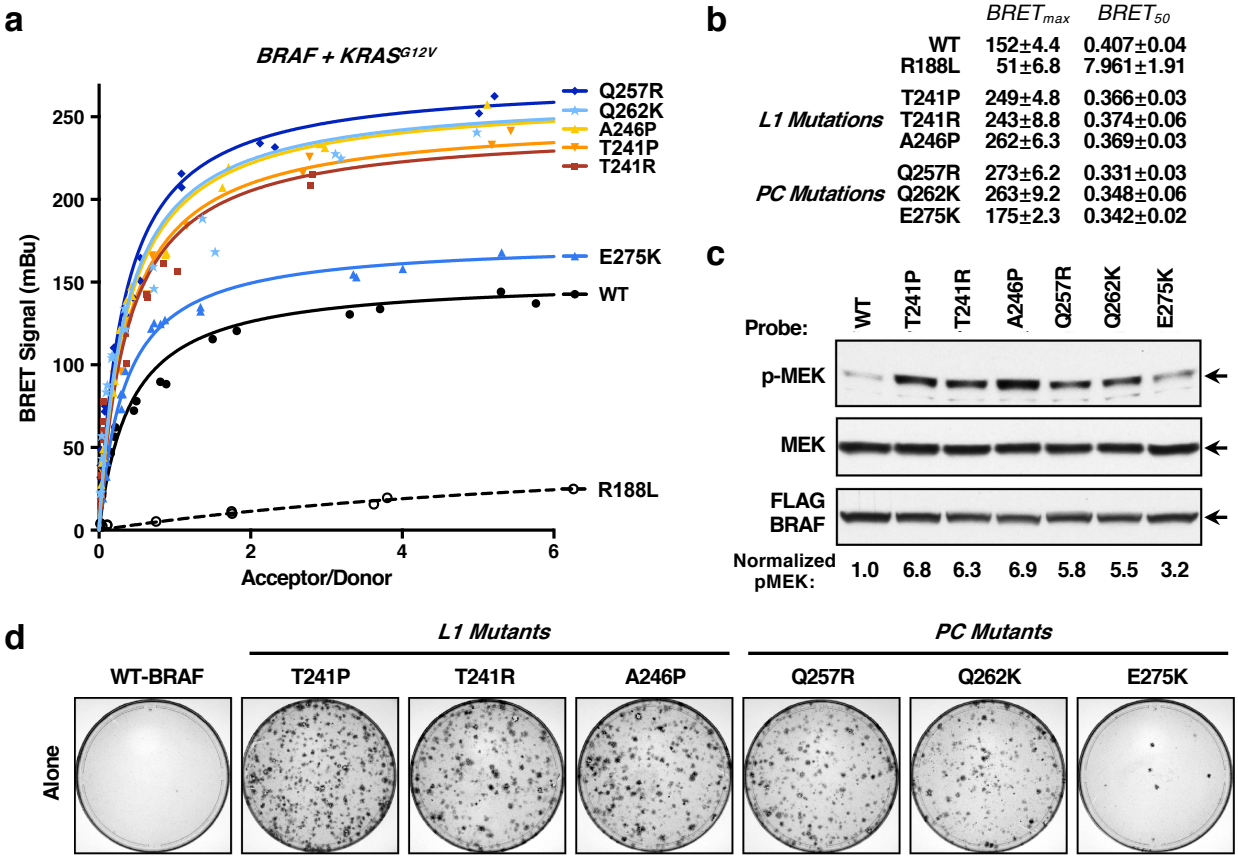
a
BRAF + KRASG12V
BRET Signal (mBu)
Acceptor/Donor
Q257R
Q262K
A246P
T241P
T241R
E275K
WT
R188L
b
BRETmax BRET50
WT 152±4.4 0.407±0.04
R188L 51±6.8 7.961±1.91
L1 Mutations
T241P 249±4.8 0.366±0.03
T241R 243±8.8 0.374±0.06
A246P 262±6.3 0.369±0.03
PC Mutations
Q257R 273±6.2 0.331±0.03
Q262K 263±9.2 0.348±0.06
E275K 175±2.3 0.342±0.02
c
Probe:
WT
T241P
T241R
A246P
Q257R
Q262K
E275K
p-MEK
MEK
FLAG BRAF
Normalized pMEK:
1.0 6.8 6.3 6.9 5.8 5.5 3.2
d
L1 Mutants
PC Mutants
WT-BRAF
T241P
T241R
A246P
Q257R
Q262K
E275K
Alone

Figure 4

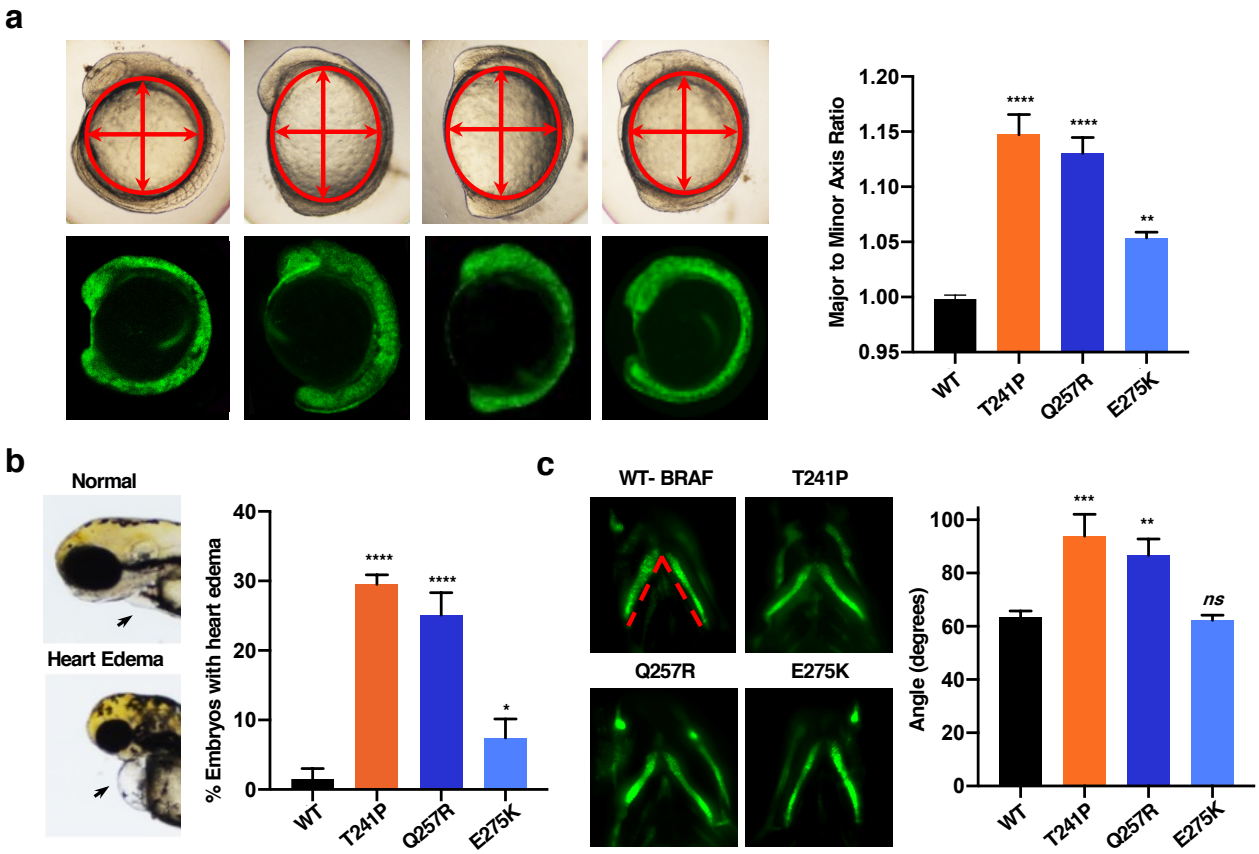

d

Alteration	T241P	All Class A	Q257R	All Class B	E275K Class C
Hypotonia	3/3 (100%)	5/7 (71%)	10/10 (100%)	10/10 (100%)	1/1 (100%)
Developmental delay	3/3 (100%)	10/10 (100%)	14/14 (100%)	15/15 (100%)	0/1
Cardiomyopathy	1/3 (33%)	3/9 (33%)	8/17 (47%)	8/17 (47%)	0/1
Cardiovascular malformation	3/3 (100%)	7/10 (70%)	12/17 (70%)	13/18 (72%)	1/1 (100%)
Short stature	3/3 (100%)	10/10 (100%)	15/15 (100%)	16/16/ (100%)	0/1
Dysmorphic facial features	3/3 (100%)	10/10 (100%)	12/12 (100%)	13/13 (100%)	1/1 (100%)
Downslanting palpebral fissures	1/1 (100%)	7/7 (100%)	5/5 (100%)	5/5 (100%)	0/1
Hypertelorism	1/1 (100%)	6/6 (100%)	2/2 (100%)	2/2 (100%)	0/1
Ectodermal abnormalities	3/3 (100%)	9/10 (90%)	17/17 (100%)	18/18 (100%)	1/1 (100%)

Figure 5

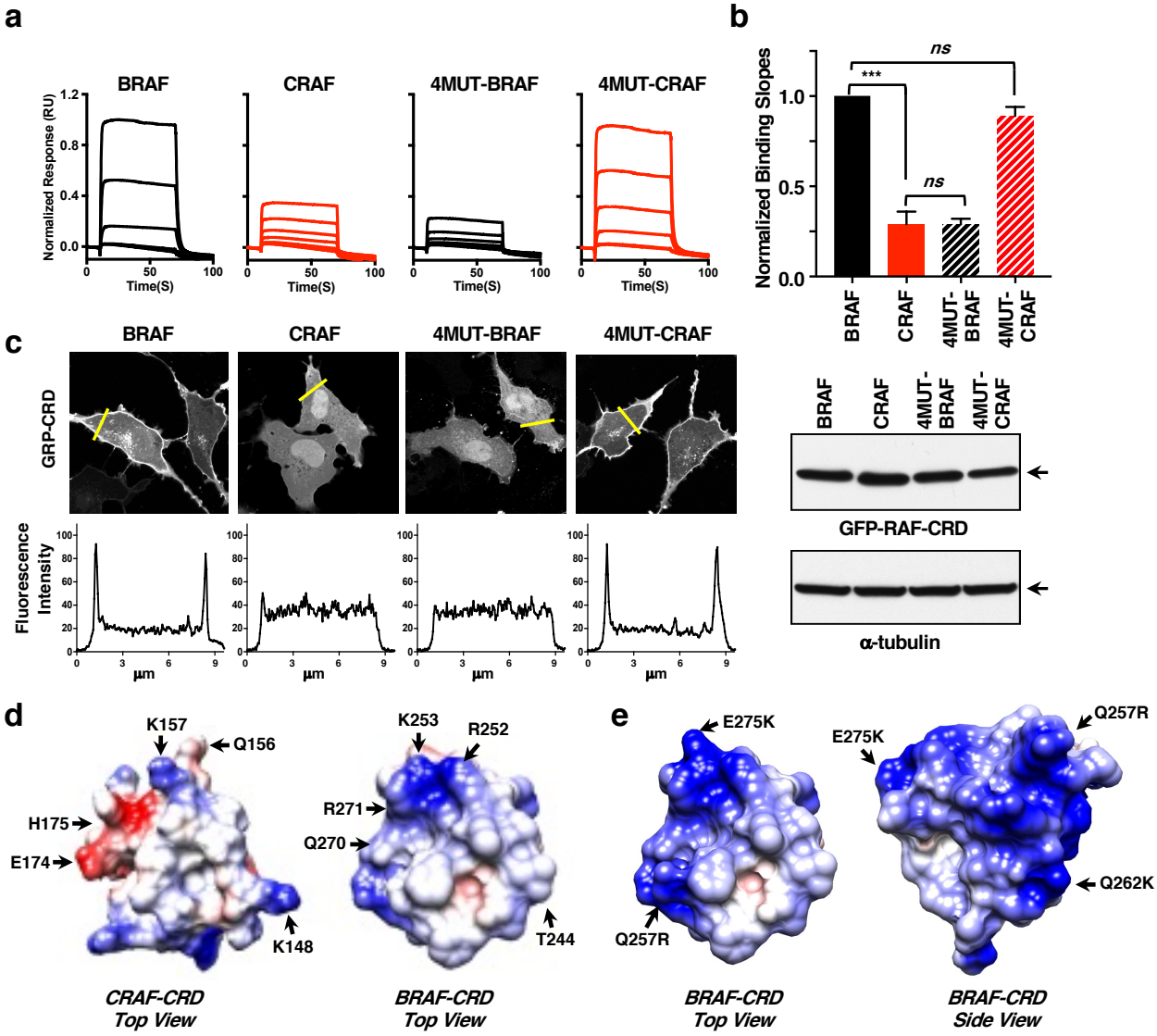
a
BRAF
CRAF
4MUT-BRAF
4MUT-CRAF
Normalized Response (RU)
Time(S)
b
Normalized Binding Slopes
ns
***
ns
BRAF
CRAF
4MUT-BRAF
4MUT-CRAF
c
GRP-CRD
Fluorescence Intensity
µm
GFP-RAF-CRD
α-tubulin
d
K157
Q156
H175
E174
K148
K253
R252
R271
Q270
T244
CRAF-CRD Top View
BRAF-CRD Top View
e
E275K
Q257R
E275K
Q257R
Q262K
BRAF-CRD Top View
BRAF-CRD Side View

Figure 6

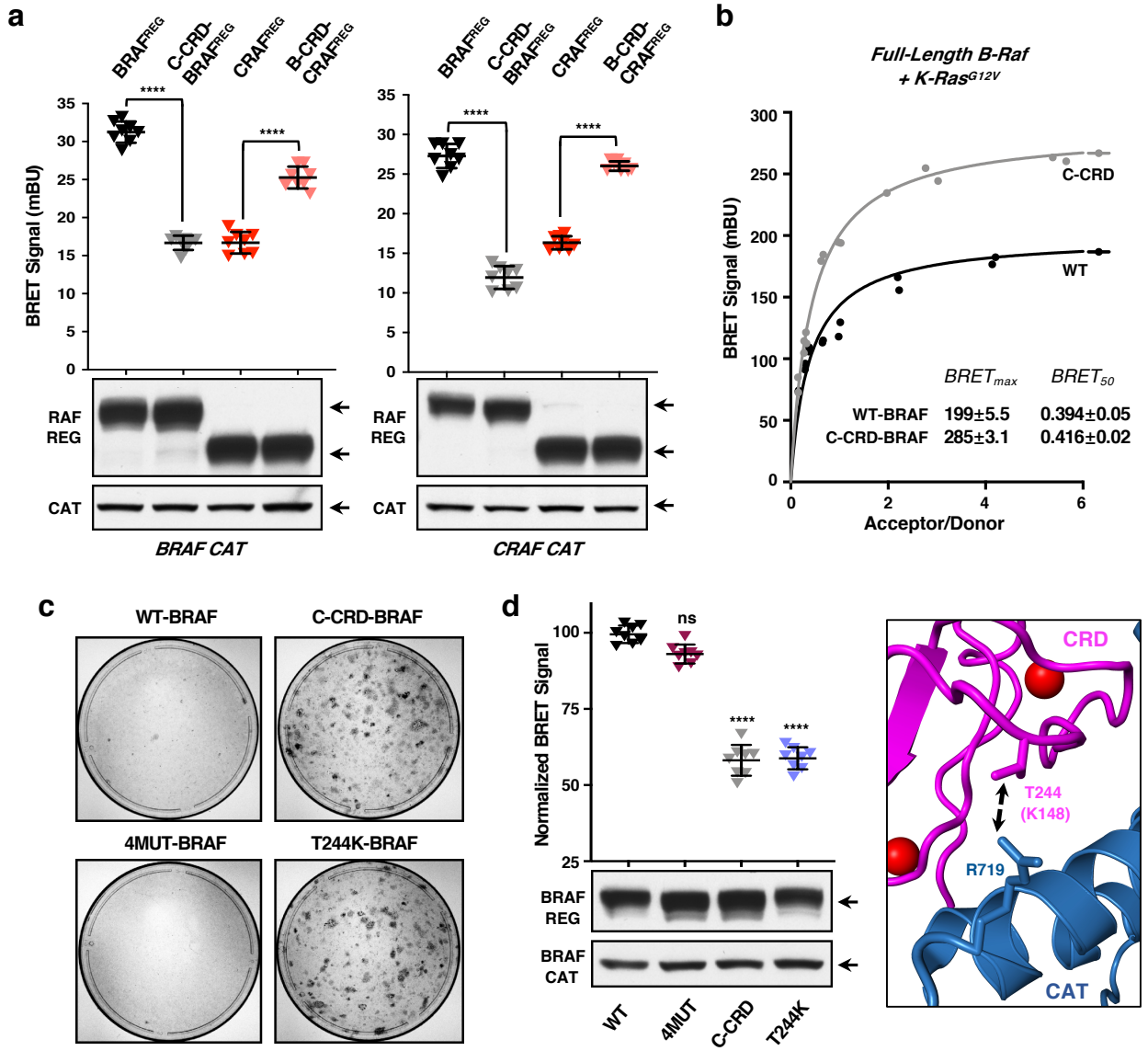
a
BRAFREG
C-CRD-BRAFREG
CRAFREG
B-CRD-CRAFREG
BRET Signal (mBU)
****
RAF REG
CAT
BRAF CAT
CRAF CAT
b
Full-Length B-Raf + K-RasG12V
C-CRD
WT
BRET Signal (mBU)
Acceptor/Donor
BRETmax BRET50
WT-BRAF 199±5.5 0.394±0.05
C-CRD-BRAF 285±3.1 0.416±0.02
c
WT-BRAF
C-CRD-BRAF
4MUT-BRAF
T244K-BRAF
d
Normalized BRET Signal
ns
BRAF REG
BRAF CAT
WT
4MUT
C-CRD
T244K
CRD
T244 (K148)
R719
CAT

Figure 7

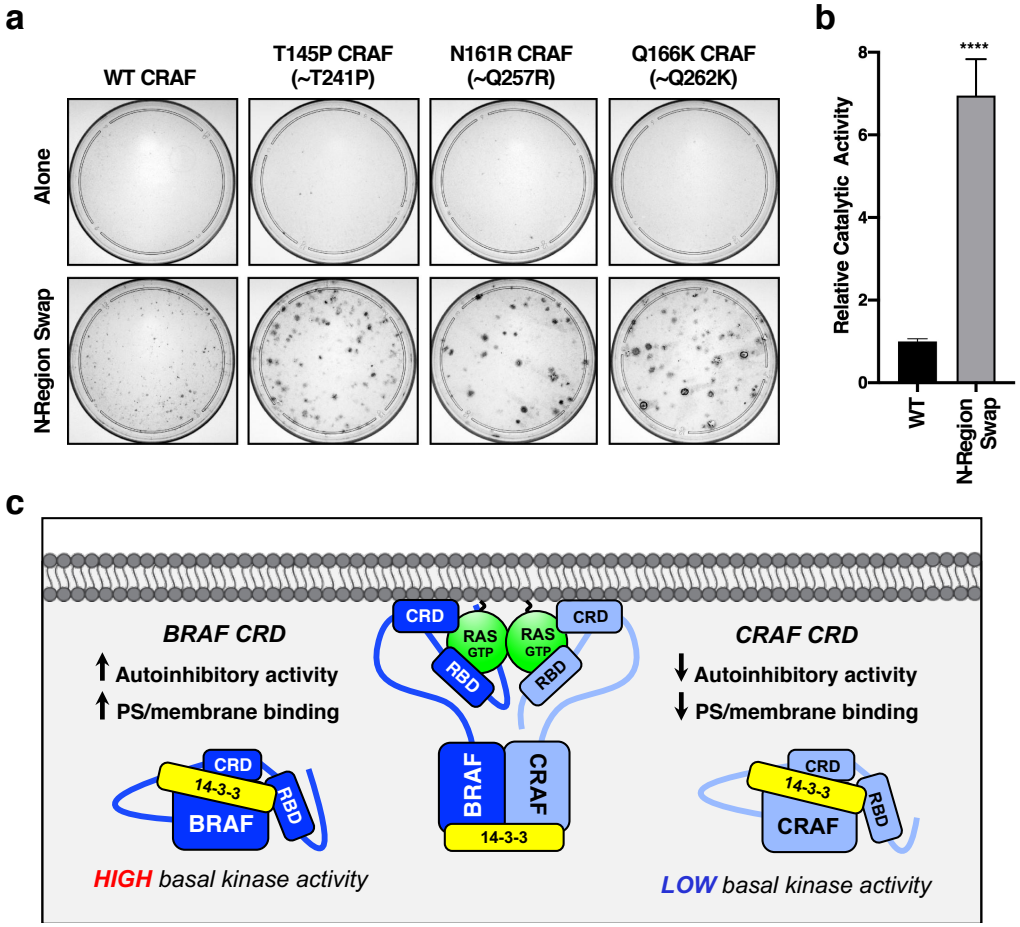
a
WT CRAF
T145P CRAF (~T241P)
N161R CRAF (~Q257R)
Q166K CRAF (~Q262K)
Alone
N-Region Swap
b
Relative Catalytic Activity
****
WT
N-Region Swap
c
BRAF CRD
Autoinhibitory activity
PS/membrane binding
CRD
14-3-3
RBD
BRAF
HIGH basal kinase activity
CRD
RAS GTP
RAS GTP
RBD
RBD
CRD
BRAF
CRAF
14-3-3
CRAF CRD
Autoinhibitory activity
PS/membrane binding
CRD
14-3-3
RBD
CRAF
LOW basal kinase activity

Supplementary Data

Supplementary Fig. 1

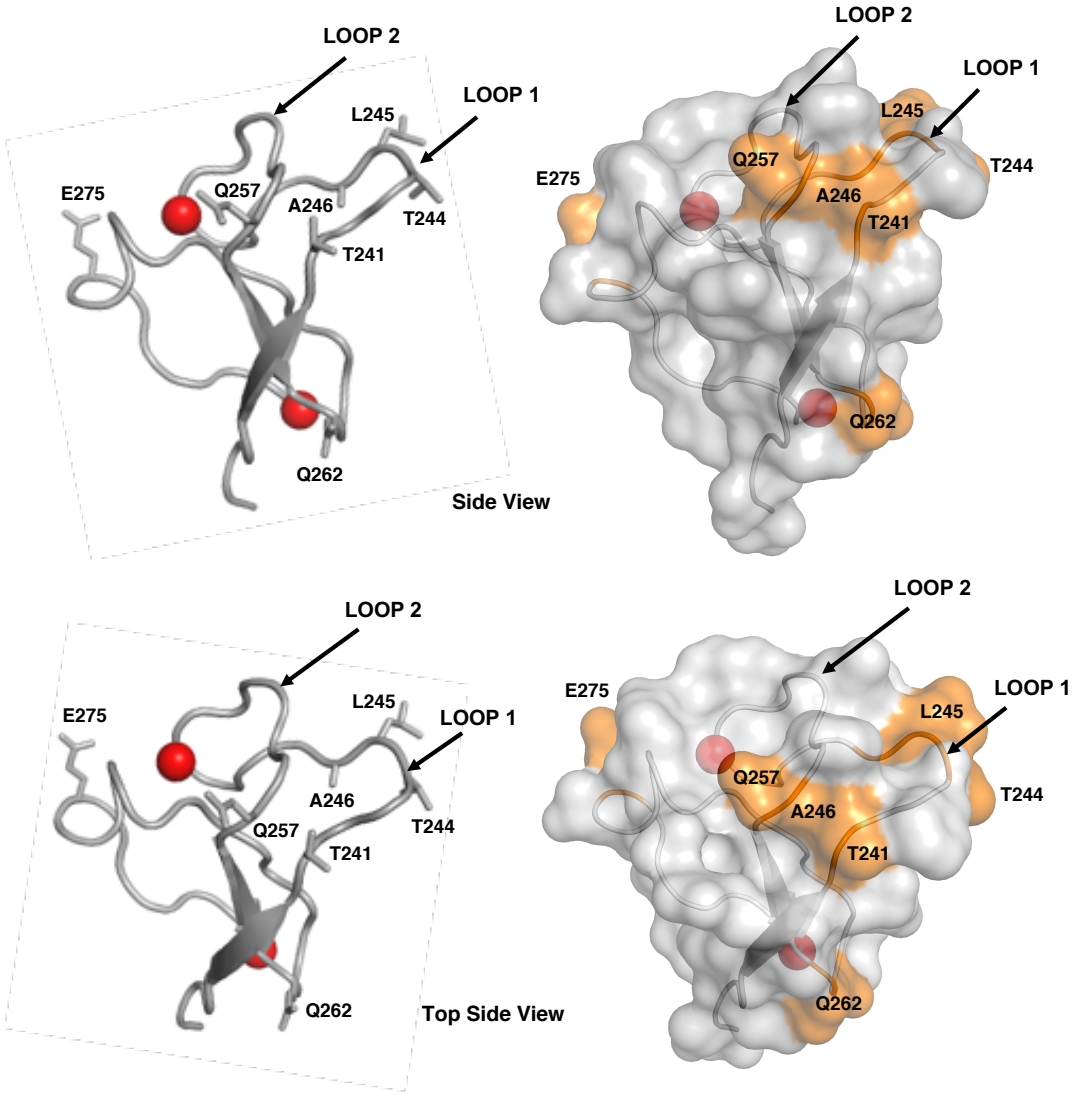

Supplementary Fig. 1. RASopathy-associated BRAF-CRD mutations.

Ribbon (left) and space filling (right) diagrams of the BRAF CRD with the two Zn^{2+} ions coordinated in the CRD depicted as red spheres. CRD residues mutated in the RASopathies are labeled and shown in orange in the space filling diagram and their side chains are shown (PDB: 6NYB) in the ribbon diagram.

Supplementary Fig. 2

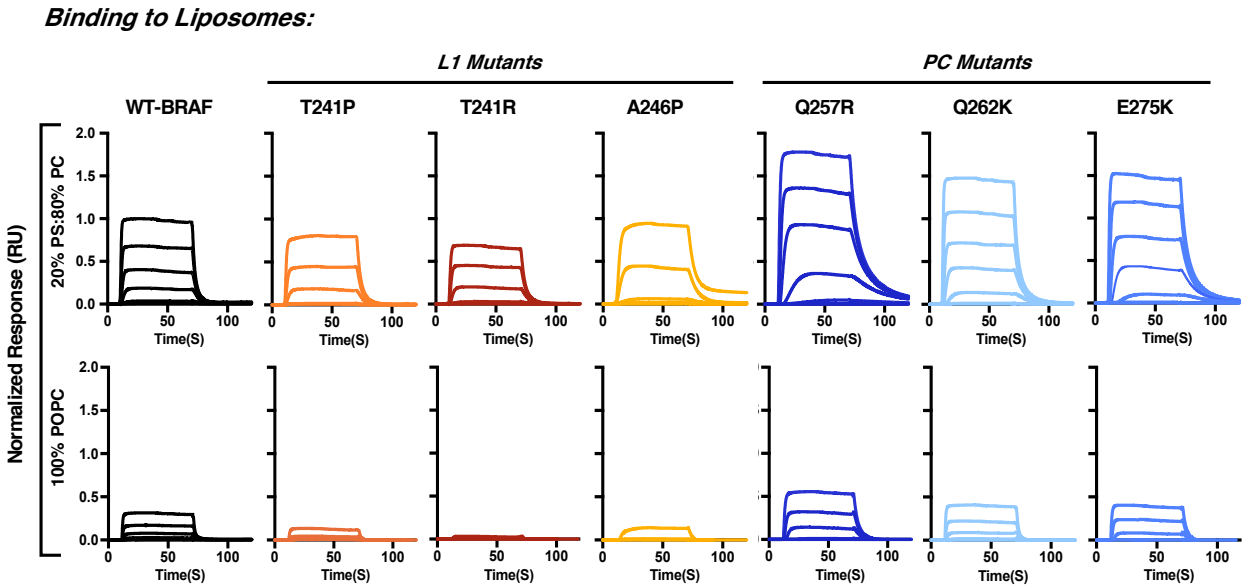

Supplementary Fig. 2. Effect of RASopathy-associated BRAF-CRD mutations on PS binding. A 2-fold dilution series of purified 5μM WT or mutant BRAF-CRD proteins was injected over liposomes containing 20% POPS/80% POPC or 100% POPC, and binding responses were determined by SPR. Sensorgrams were normalized to the WT-BRAF-CRD binding response. Binding responses are representative of 3 independent experiments with similar results.

Supplementary Fig. 3

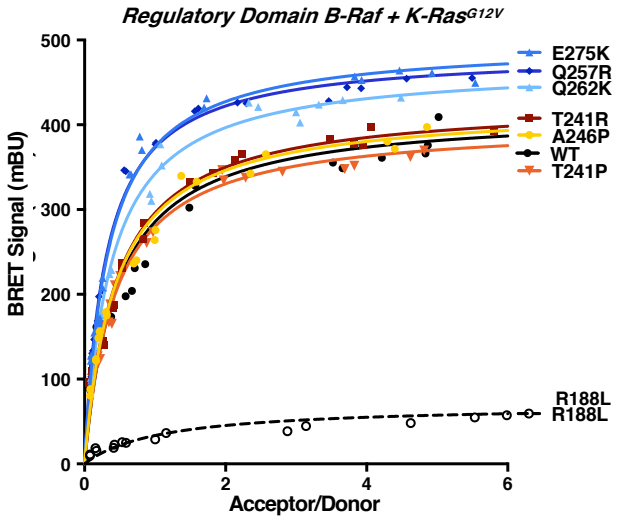

		$BRET_{max}$	$BRET_{50}$
	WT	416±6.7	0.448±0.04
	T241P	402±4.9	0.438±0.02
L1 Mutations	T241R	427±9.4	0.445±0.04
	A246P	422±8.5	0.440±0.03
	Q257R	486±5.5	0.303±0.02
PC Mutations	Q262K	471±7.0	0.377±0.02
	E275K	497±7.9	0.330±0.02

Supplementary Fig. 3. Effect of RASopathy-associated BRAF-CRD mutations on binding of $BRAF^{REG}$ to $KRAS^{G12V}$ in live cells. a BRET saturation curves are shown examining the interaction of WT or mutant $BRAF^{REG}$-RLuc8 proteins with Venus-$KRAS^{G12V}$. $BRET_{max}$ and $BRET_{50}$ values are also listed ± standard error. Of note, expression levels of the donor and acceptor constructs were monitored and are incorporated into the calculations determining the $BRET_{max}$ and $BRET_{50}$ values as described in the methods. Saturation curves were repeated three times with similar results.

Supplementary Fig. 4

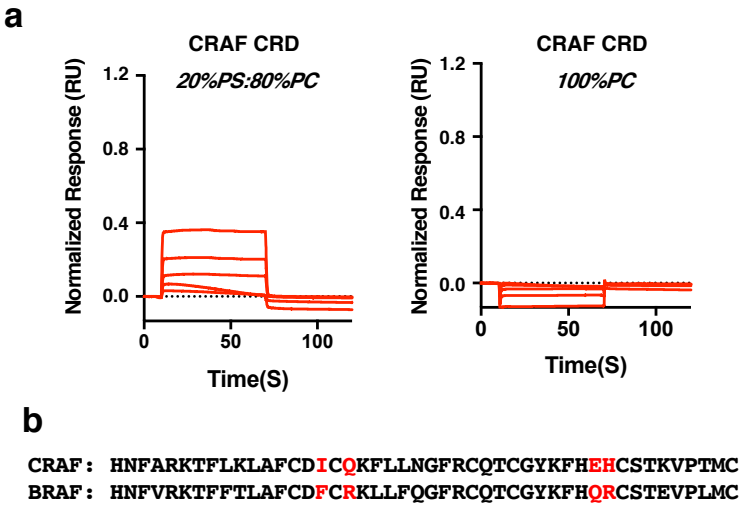

Supplementary Fig. 4. The CRAF CRD exhibits preferential binding to PS containing nanodics. **a** A 2-fold dilution series of purified 5μM CRAF-CRD was injected over nanodiscs containing 20% POPS/80% POPC or 100% POPC, and binding responses were determined by SPR. **b** Shown is the sequence alignment of the BRAF and CRAF-CRDs with the 4MUT residues shown in red.

Supplementary Table 1

		L1 Mutations			*PC Mutations*		
	WT	T241P	T241R	A246P	Q257R	Q262K	E275K
PS Binding	Yes	~ to WT	~ to WT	~ to WT	↑	↑	↑
Autoinhibition	Yes	↓	↓	↓	↓	↓	~ to WT
CLASS		A	A	A	B	B	C
$KRAS^{G12V}$ binding FL-BRAF (BRET)	Yes	↑↑ Levels	↑↑ Levels	↑↑ Levels	↑↑ Levels ↑ Affinity	↑↑ Levels ↑ Affinity	↑ Levels ↑ Affinity
$KRAS^{G12V}$ binding REG-BRAF (BRET)	Yes	~ to WT	~ to WT	~ to WT	↑ Levels ↑ Affinity	↑ Levels ↑ Affinity	↑ Levels ↑ Affinity
Transformation	No	Yes	Yes	Yes	Yes	Yes	Yes (Weaker)
Zebrafish Defects	No	Yes	nd	nd	Yes	nd	Yes (Weaker)

Class A – mutation relieves autoinhibition
Class B – mutation relieves autoinhibition and enhances PS binding.
Class C – mutation enhances PS binding but has no effect on autoinhibition

Supplementary Table 1. Summary and classification of RASopathy-associated BRAF-CRD mutations.

Supplementary Table 2

Protein	Foci # (±SEM)
WT-BRAF	0
T241P-BRAF	277±17
T241R-BRAF	236±12
A246P-BRAF	253±13
Q257R-BRAF	219±15
Q262K-BRAF	165±10
E275K-BRAF	8±3
WT BRAF	6±2
C-CRD-BRAF	155±25
4MUT-BRAF	3±2
T244K-BRAF	143±22
WT-CRAF	0
CRAF(B-N region)	1±2 (small foci)*
T145P-CRAF	1±2 (small foci)
T145P (B-N region)	84±11
N161R CRAF	1±1 (small foci)
N161R (B-N region)	52±7
Q166K-CRAF	0
Q166K (B-N region)	67±8

* Also observe numerous clusters of 5-10 cells

Supplementary Table 2. Quantification of focus forming assays. Foci number represent the number of foci observed on a monolayer of NIH-3T3 cells in a 10 cm dish. Numbers represent the average number of foci observed in at least 2 independent experiments ± standard error.

Supplementary Table 3. Reported evaluations of patients with BRAF-CRD mutations. See attached Excel file.